THE ASTROPHYSICAL JOURNAL, 369:147–156, 1991 March 1

THE FORMATION OF OXYGEN-CONTAINING ORGANIC MOLECULES IN THE ORION COMPACT RIDGE

T. J. MILLAR[1], ERIC HERBST,[2] AND S. B. CHARNLEY[3]

Received 1990 May 31; accepted 1990 August 20

ABSTRACT

Following a suggestion of Blake et al., we have attempted to account for the unusually large abundances of selected oxygen-containing organic molecules in the so-called "compact ridge" source directed towards Orion KL by a gas-phase chemical model in which large amounts of water are injected into the source from the IRc2 outflow. Although our quantitative model results show that the calculated abundances of methanol, methyl formate, and dimethyl ether can be enhanced relative to their values in the absence of water injection, the enhancements fall far short of explaining the very large observed abundances of these species. Models in which methanol is injected rather than water are more successful, although the source of the methanol is unclear.

Subject headings: interstellar: abundances — interstellar: molecules — molecular processes

1. INTRODUCTION

In recent years, small ($\approx$0.1 pc), dense ($n \approx 10^7$ cm^{-3}), hot ($T \approx$ 100–200 K) clumps have been detected in star-forming molecular clouds (Sweitzer 1978; Pauls et al. 1983; Henkel et al. 1987; Walmsley et al. 1987; Jacq et al. 1990). These regions can contain much larger abundances of certain polyatomic molecules than those found in cold, dark clouds (Walmsley 1989). In particular, the Orion Molecular Cloud appears to contain two such clumps in the direction of the Kleinman-Low Nebula—the hot core and the compact ridge (Blake et al 1987). Although there are several similarities involving density, temperature, and size between these regions, there are also some striking differences in chemical abundances (Blake et al. 1987; Irvine, Goldsmith, & Hjalmarson 1987). The hot core contains large abundances of nitrogen-bearing and relatively saturated (hydrogen-rich) molecules such as HDO, NH_3, NH_2D, CH_3OH, CH_2CHCN, and CH_3CH_2CN, while SO and SO_2 are underabundant. In addition to HDO, the compact ridge source contains large abundances of oxygen-bearing molecules such as CH_3OH, CH_2CO, CH_3OCH_3, $HCOOCH_3$, and HCOOH. These chemical differences have led to the suggestion that the two clumps have had different evolutionary behavior, although both are very close to the luminous infrared source, IRc2, which has an oxygen-rich outflow, the so-called Plateau source. The hot core is thought to have been formed as a clump left over from the star-formation process and is now heated by infrared radiation from IRc2. A chemical model of this region incorporating gas-phase reactions, accretion onto the dust, and surface reactions involving H and D atoms, in a cloud undergoing free-fall collapse has been developed recently (Brown, Charnley, & Millar 1988; Brown & Millar 1989a, b). This model can account at least qualitatively for the enhanced abundances of NH_3, HDO, and NH_2D among other species seen in the hot core source. Enhanced abundances of these species are produced via H atom and D atom sticking reactions on dust grains followed by thermal desorption due to the heat from IRc2.

Because of the number of oxygen-bearing molecules in the compact ridge and its position on the northern edge of the southern molecular ridge cloud in Orion, it has been suggested that the compact ridge has formed in the interaction of the oxygen-rich outflow from IRc2 and the quiescent extended ridge cloud (Blake et al. 1987). In addition to the large oxygen-containing molecules seen in this source, detailed isomeric effects also occur. For example, although dimethyl ether (CH_3OCH_3) and methyl formate ($HCOOCH_3$) have been detected, their respective isomers ethanol (CH_3CH_2OH) and acetic acid (CH_3COOH) have not. Blake et al. (1987) have suggested that the enhanced abundances and isomeric effects are the direct result of the injection of water from the outflow into the southern ridge cloud. In particular, their specific route to oxygen-containing organic molecules commences with the radiative association reaction

$$CH_3^+ + H_2O \rightarrow CH_3OH_2^+ + h\nu\,, \qquad (1)$$

which leads to methanol upon dissociative recombination with electrons, while the reaction

$$CH_3OH_2^+ + H_2CO \rightarrow H_2COOCH_3^+ + H_2 \qquad (2)$$

leads to methyl formate (and not acetic acid) upon dissociative recombination. Furthermore, the binary reaction

$$CH_3OH_2^+ + CH_3OH \rightarrow (CH_3)_2OH^+ + H_2O \qquad (3)$$

leads to dimethyl ether (and not ethanol) upon dissociative recombination. Such a scheme, when incorporated into a simple steady state analysis of abundance ratios, appears to account for many of the chemical properties of the compact ridge cloud. It is important, however, to test the suggested reaction scheme with a more detailed model calculation which accounts for time dependence, actual abundances rather than abundance ratios, and a more detailed chemistry which includes the radiative association

$$CH_3^+ + CH_3OH \rightarrow (CH_3)_2OH^+ + h\nu\,, \qquad (4)$$

[1] Department of Mathematics, University of Manchester Institute of Science and Technology, P.O. Box 88, Manchester M60 1QD, U.K.
[2] Department of Physics, Duke University, Durham, NC 27706.
[3] Max-Planck-Institut für Physik und Astrophysik, Institut für extraterrestrische Physik, and Department of Physics, Rensselaer Polytechnic Institute. Postal Address: Space Science Division, NASA Ames Research Center, Moffett Field, CA 94035.

which is another mechanism leading to formation of dimethyl ether (Herbst 1987). In addition, it is exceedingly important to be sure that the main depletion reactions of CH_3^+, involving H_2, H_2O, and electrons are described adequately. Neglect of the reactions between CH_3^+ and H_2 or electrons could lead to a serious overestimate of the methyl ion abundance and hence those of methanol and other oxygen-containing organic molecules.

In this paper, we therefore report the results of calculations in which a large abundance of water is injected into a molecular cloud having properties resembling the southern ridge cloud, i.e., $n = 2 \times 10^5$ cm^{-3} and $T = 70$ K. To derive the unperturbed abundances in the southern ridge cloud, we have first performed a pseudo–time-dependent study in which the chemistry of several large oxygen-bearing molecules has been included. The basic chemistry has been described by Millar, Leung, & Herbst (1987) and Millar et al. (1988). Secondly, in addition to the *in situ* formation of H_2O, we have included a term describing the injection of water molecules. Although we have formally calculated abundances over a period of 10^8 yr, the lifetime of the Compact Ridge must be much shorter than this and we shall concentrate on results for times $\leq 3 \times 10^6$ yr after the injection has begun.

In the following section, the reactions and rate coefficients governing the formation of large oxygen-containing species are discussed in detail. In addition to these reactions, we have included destruction reactions involving the abundant ions H^+, He^+, C^+, H_3^+ HCO^+, H_3O^+, some of which have already been studied in the laboratory.

2. THE CHEMICAL MODEL

In ion-molecule syntheses of neutral interstellar molecules, precursor ions of greater complexity are formed initially. These ions normally contain one or two hydrogen atoms more than the final neutral products, which are produced in dissociative recombination processes. Although some experimental work on the products of dissociative recombination reactions has recently been accomplished (Herd, Adams, & Smith 1990), in general it is still necessary to estimate branching ratios for such products. In our past calculations we have based these branching ratios on the simple idea of Green & Herbst (1979), that ejection of one or more hydrogen atoms from the parent neutral species is preferred, and have customarily assigned equal probabilities to channels in which one hydrogen atom is removed, and in which two such atoms (or an H_2 molecule) are removed. A discussion of other approaches is given by Herbst (1988) and the sensitivity of model results to these different approaches has been given by Millar et al. (1988). The approach we customarily take cannot be used for some of the protonated ions of the oxygen-bearing organic species in our model because the heavy neutral molecules remaining when two hydrogen atoms are removed are not in the model. In such cases, we have always put in a replacement channel involving the breaking of a single bond so that two product channels are available. For example, the dissociative recombination of protonated dimethyl ether proceeds equally via the two channels

$$(CH_3)_2OH^+ + e \rightarrow CH_3OCH_3 + H \quad (5a)$$

$$\rightarrow CH_3OH + CH_3 . \quad (5b)$$

Such an assumption, though somewhat arbitrary, ensures that artificially large abundances do not result from recycling, in which neutral species, protonated by reactions with abundant ions such as H_3^+ and HCO^+, simply reform via dissociative recombination (Millar, Leung, & Herbst 1987).

Reaction (1), the radiative association between CH_3^+ and H_2O, is thought to be central to methanol formation in molecular clouds and accounts for the methanol abundance in TMC-1, for example, at early time (see, e.g., the "standard" model of Herbst & Leung 1989). However, the calculated and observed fractional abundances of methanol in TMC-1 are only a few $\times 10^{-9}$, which is considerably below the observed fractional abundance in the compact ridge. The idea of Blake et al. (1987) is that sufficient water injected into the compact ridge will lead to an enhanced abundance of methanol via reaction (1) and dissociative recombination. In our model, we use a newly calculated value for the rate coefficient of this radiative association of 2.95×10^{-13} $(T/300)^{-3.4}$ cm^3 s^{-1}. This formula pertains only in the temperature range $\approx$70–300 K; at lower temperatures the inverse temperature dependence weakens considerably (Herbst 1985). The newly calculated value has been obtained via the phase-space technique (Herbst 1987) with the assumption that the radiative stabilization rate of the complex is 10^3 s^{-1}. If the mechanism of complex stabilization is via emission of radiation within the ground electronic state, this value represents an upper limit. The theoretical value can be partially checked by comparison with experimental data at 225 and 300 K in the high-pressure limit in which the association proceeds via a partially saturated collisional stabilization (Bates & Herbst 1988; Smith & Adams 1978).

The calculation of the radiative association rate coefficient for this basic process has been undertaken with the assumption that the rotational energy levels of the reactants in the compact ridge are in thermal equilibrium. Although this approximation is certainly valid for the methyl ion, which does not possess a permanent dipole moment, it is of more questionable validity for water, which possesses large Einstein A-coefficients for rotational emission. If the rotational levels of water are considerably cooler than the kinetic temperature of the source, then the calculated rate coefficient increases considerably, by up to one order of magnitude if water is primarily in its lowest state. However, the large optical depths for water in this source as well as the infrared radiation undoubtedly present indicate to us that thermal equilibrium is a reasonable approximation here. In addition, it should be noted that Blake et al. (1987) assume HDO to be thermalized in the compact ridge.

Protonated methyl formate ($H_2COOCH_3^+$) is formed via reaction (2) in our model. Recent laboratory work on this reaction, first proposed by Blake et al. (1987), indicates that the products of the reaction are $CH_3OCH_2^+ + H_2O$ with a small rate coefficient of 2.1×10^{-11} cm^3 s^{-1} at 320 K (Ikezoe et al. 1987). Work in progress (Bohme 1990) indicates, on the contrary, that protonated methyl formate is indeed a product of this reaction. Often, ion-molecule reactions with small rate coefficients at room temperature possess larger rate coefficients at lower temperature (see, e.g., Bass et al. 1983; Wlodek et al. 1990), especially if the potential surfaces contain bottlenecks in the output channels. For the sake of comparison with the results of Blake et al. (1987) we retain their assumed products ($H_2COOCH_3^+ + H_2$) and rate coefficient of $\approx 10^{-9}$ cm^3 s^{-1}.

Reactions (3) and (4) lead to protonated dimethyl ether, $(CH_3)_2OH^+$. Reaction (3), a normal ion-molecule reaction, has been studied in the laboratory by Bass et al. (1983) at temperatures in excess of 200 K. It is one of those ion-molecule reactions which, although slow at room temperature, increases as temperature is decreased. We have used the phase-space

technique (Bass et al. 1983; Herbst 1987; Wlodek et al. 1990) to calculate the rate coefficient at 100 K to be 4.5×10^{-10} cm^3 s^{-1}. Reaction (4) is a radiative association reaction, and we have previously calculated its rate coefficient to be 7.8×10^{-12} $(T/300)^{-1.1}$ cm^3 s^{-1} in the range 10–50 K (Herbst 1987). An extension of this formula to 100 K is not unreasonable.

Three other large protonated oxygen-containing organic molecules in our model are protonated acetaldehyde, CH_3CHOH^+, protonated ethanol, $C_2H_5OH_2^+$, and protonated acetone $(CH_3)_2COH^+$. Their syntheses do not involve methanol or its protonated ion and will not be enhanced directly via reaction (1) when water is mixed into the source. These ions form acetaldehyde, ethanol, and acetone, respectively, upon dissociative recombination with electrons. Protonated acetaldehyde is thought to form via the radiative association reaction

$$H_3O^+ + C_2H_2 \rightarrow CH_3CHOH^+ + h\nu \,. \quad (6)$$

Recently, Herbst et al. (1989) have studied the corresponding three-body association in the laboratory in a SIFT apparatus and used the result to infer the radiative association rate coefficient in the 10–50 K range. Using a similar analysis, we infer that the rate coefficient for reaction (6) is very much slower than in models in the literature published before the work of Herbst et al. (1989), and the corresponding acetaldehyde abundance is considerably lower.

In our model, protonated ethanol is formed via the radiative association reaction (Herbst 1987)

$$H_3O^+ + C_2H_4 \rightarrow C_2H_5OH_2^+ + h\nu \,. \quad (7)$$

This reaction has also been studied recently under three-body conditions via the SIFT technique (Herbst et al. 1989) and the result used to infer a radiative association rate coefficient in the 10–50 K range. The inferred value is in close agreement with an earlier purely theoretical value (Herbst 1987). For the temperature range 50–300 K, we infer a radiative association rate coefficient of $1.3 \times 10^{-14} (T/300)^{-3.0}$ cm^3 s^{-1}.

Finally, Combes et al. (1987) have suggested that protonated acetone (CH_3COCH_3) is formed via the radiative association reaction

$$CH_3^+ + CH_3CHO \rightarrow (CH_3)_2CHO^+ + h\nu \quad (8)$$

in order to explain the observed abundance of acetone in Sgr B2. We have used the phase-space technique to estimate the rate coefficient for reaction (8), which competes with several exothermic channels. Our value is 5.7×10^{-11} $(T/300)^{-0.66}$ cm^3 s^{-1} in the range 10–300 K. More recently, Herbst, Giles, & Smith (1990) have used SIFT data in the three-body pressure range to refine the calculated value and estimate its uncertainty.

3. MODEL RESULTS

In this section, the results of several calculations are reported in which either water or methanol is injected into a molecular cloud. In order to discuss any abundance enhancements obtained by this process, we begin by reporting the calculations of the unperturbed abundances under the fixed physical conditions $n(H_2) = 10^5$ cm^{-3} and $T = 70$ K. These conditions pertain to the extended ridge cloud rather than to the compact ridge source. The initial elemental abundances of O, C, and N with respect to H_2 are taken to be 3.52×10^{-4}, 1.46×10^{-4}, and 4.28×10^{-5}, respectively.

3.1. *Unperturbed Model*

We have incorporated the specific reactions discussed in § 2 into a pseudo–time-dependent chemical kinetic model. The basic chemistry has been discussed previously for dark cloud models (Millar et al. 1987; Millar et al. 1988) but has been extended by about 100 reactions in order to account accurately for the formation and depletion of the oxygen-bearing organic molecules. In models of this type, in which the elemental oxygen abundance exceeds the elemental carbon abundance, the abundances of all large molecules peak at so-called "early times before declining to steady state values at a time $\geq 10^7$ yr. Our specific results for the fractional abundances of selected species with respect to the H_2 density at times of 1.6×10^5, 5.0×10^5, 7.9×10^5, and 3.2×10^6 yr are shown in Table 1, alongside observed fractional abundances for the compact ridge, taken mainly from Blake et al. (1987). The theoretical results at 1.6×10^5 yr are essentially the maximum fractional abundances which the oxygen-bearing organic molecules obtain.

Unlike the case of the well-studied dark cloud TMC-1 (Herbst & Leung 1989, 1990), where peak abundances and observations are in good agreement, the peak calculated abundances of the complex molecules in our model tend to be significantly smaller than the observed compact ridge values. Ketene (CH_2CO) is an obvious exception to this generalization; its large calculated fractional abundance in the model is due to the inclusion of the unstudied reaction

$$C_2H_4^+ + O \rightarrow CH_3CO^+ + H \,, \quad (9)$$

for which we know neither the reaction rate (10^{-10} cm^3 s^{-1} is adopted here) nor the products formed (Herbst & Leung 1989). If this reaction is excluded from the model, the fractional peak abundance of ketene is reduced to 2×10^{-9}, at which time its protonated precusor is formed by the radiative association reaction

$$CH_3^+ + CO \rightarrow CH_3CO^+ + h\nu \,. \quad (10)$$

The calculated fractional abundance of methanol is never larger than 10^{-9}, compared with the observed value of $\approx 10^{-7}$. This is due to the inefficient conversion of methyl ion into $CH_3OH_2^+$ because the former ion is lost predominantly via reactions with H_2, atomic oxygen, and electrons. If the small rate coefficient for the radiative association reaction between methyl ion and water is raised several orders of magnitude to a value of 2×10^{-9} cm^{-3} s^{-1}, we calculate that the observed fractional abundance of methanol can be duplicated at "early time." Such a large rate coefficient is unlikely, both theoretically and since it would lead to an overproduction of methanol in cooler dark clouds, unless the water were depleted in such sources (Langer & Glassgold 1990). To maximize the methyl ion abundance, we have used a low value for the rate coefficient of the radiative association between $CH_3^+ + H_2$ of $1.3 \times 10^{-14} (T/300)^{-1}$ in the temperature range 10–100 K (Smith 1989), which is in agreement with the very recent 80 K measurement by Gerlich & Kaefer (1989).

Although the peak calculated methanol fractional abundance in Table 1 is significantly below the observed value, the situation is far worse for the larger oxygen-containing molecules—methyl formate and dimethyl ether—detected in the compact ridge source. Our peak abundances are orders of magnitude too low (see Table 1). Even if one uses rate coefficients appropriate for $T = 10$ K, i.e., by assuming that these complex molecules have been formed previously in a cold gas,

TABLE 1

SELECTED FRACTIONAL ABUNDANCES OF UNPERTURBED MODEL

SPECIES	FRACTIONAL ABUNDANCES				
	1.6×10^5 yr	5.0×10^5 yr	7.9×10^5 yr	3.2×10^6 yr	Observed[a]
C	1.1(−05)	1.1(−09)	7.2(−11)	2.4(−12)	
O	2.3(−04)	1.6(−04)	1.2(−04)	3.7(−05)	
N	3.9(−05)	2.2(−05)	1.2(−05)	8.9(−07)	
O_2	2.3(−07)	2.5(−05)	4.3(−05)	8.4(−05)	
N_2	1.7(−06)	1.0(−05)	1.5(−05)	2.1(−05)	
OH	9.2(−09)	1.3(−08)	1.5(−08)	2.8(−08)	
CO	1.2(−04)	1.4(−04)	1.5(−04)	1.5(−04)	
NO	4.9(−09)	8.1(−09)	1.1(−08)	2.0(−08)	
H_2O	1.2(−06)	7.2(−07)	6.0(−07)	2.6(−07)	
CO_2	2.0(−07)	1.2(−07)	7.8(−08)	9.5(−08)	
H_2CO	3.1(−07)	1.3(−08)	4.4(−09)	1.0(−09)	4(−08)[b]
CH_2CO	1.0(−07)	4.6(−09)	7.3(−10)	2.7(−11)	7(−10)
CH_3OH	9.5(−10)	1.1(−11)	3.5(−12)	5.3(−13)	1(−07)
CH_3CHO	9.3(−12)	2.8(−13)	5.5(−14)	3.7(−15)	<2(−10)
$HCOOCH_3$	1.2(−11)	1.3(−14)	8.9(−16)	2.8(−17)	9(−09)
CH_3CH_2OH	1.8(−12)	6.0(−14)	3.8(−15)	6.8(−17)	<5(−10)
CH_3OCH_3	6.0(−13)	1.7(−15)	3.0(−17)	1.1(−18)	1(−08)
CH_3COCH_3	1.8(−14)	1.4(−17)	8.8(−19)	2.0(−20)	
e	4.4(−08)	4.5(−08)	4.5(−08)	4.6(−08)	
CH_3^+	1.5(−10)	3.0(−12)	1.4(−12)	6.6(−13)	
H_3O^+	5.8(−10)	4.8(−10)	4.0(−10)	2.0(−10)	
HCO^+	2.0(−09)	3.6(−09)	4.0(−09)	5.0(−09)	
$CH_3OH_2^+$	4.6(−13)	7.1(−15)	2.6(−15)	5.0(−16)	

NOTE.—Abundances are given in the form $a(-b)$, where $a(-b)$ stands for $a \times 10^{-b}$.

[a] Blake et al. (1987) unless otherwise noted.

[b] Magnum et al. (1990).

the abundances are still far lower than those observed, as has already been concluded by Herbst (1987), who used less refined modeling calculations. It is thus necessary to modify the ion-molecule chemistry and we now consider the mixing of water into the compact ridge source as suggested by Blake et al. (1987). Another possibility is the evaporation of ice-type mantles from interstellar grains which would be expected to have similar consequences for the chemical evolution of the gas if the relevant time scales are comparable. Such an evaporation has been recently considered and utilized as part of an explanation of the chemistry of the Orion hot core (Brown et al. 1988; Brown & Millar 1989a, b). The work of these authors differs from ours, however, in two important respects: (1) they consider a very rapid desorption of grain mantles due to star formation, and (2) the desorbed material becomes part of a very dense gas in which the importance of ion-molecule reactions is reduced.

3.2. *Injection of Water*

To account for the injection process, we have added a source term to the time-dependent ordinary differential equation which describes the evolution of the water abundance, as well as a term which increases the H_2 density at a rate 10^4 times the water injection rate. There are a number of factors which govern the nature of the H_2O injection term. These include (*i*) the time, as measured in the evolution of the ridge cloud, when injection begins, (*ii*) the time at which it ends, (*iii*) whether the injection process is time-dependent or steady state, and (*iv*) the magnitude of the mixing, measured in molecules of water added per unit volume per unit time ($cm^{-3}\ s^{-1}$), which in turn depends on the mass-loss rate of IRc2, the water abundance in the outflow, the distance between IRc2 and the ridge cloud, and the extent of the compact ridge source.

If, as appears likely from models of the Orion hot core (Brown et al. 1988; Brown & Millar 1989a, b), IRc2 has formed from the same cloud as the material around it, then the ambient ridge cloud must have undergone substantial chemical evolution before the wind from IRc2 can have interacted with it. We therefore assume that a time of 10^{13} s (3.17×10^5 yr), which appears reasonable from models of the hot core, has elapsed in the chemical model of the compact ridge before water is injected, although we shall also present results for injection at $t = 0$. In addition, calculations have been performed for a third initial injection time of 3×10^{11} s. However, since the results show no difference from those for which the initial time is taken to be 0, they are not presented explicitly. The mass-loss rate of IRc2, which has a luminosity of $10^5\ L_\odot$, is large, perhaps $\approx 10^{-4}\ M_\odot\ yr^{-1}$ (Wynn-Williams et al. 1984), so that injection cannot occur for a period much longer than a few times 10^5 yr. Our model results at times much longer than this are not meaningful physically but are useful in helping to delineate the chemical processes which occur in the mixed gas. We further assume for the sake of simplicity that the injection occurs at a steady rate, that no H_2O leaves the compact ridge, and that $T = 70$ K reaction rates pertain for chemical reactions involving the injected water.

For a spherically symmetric outflow, the number of hydrogen molecules which cross unit area (cm^2) per unit time (s) is $1.5 \times 10^{10}\ [dM_{-4}/dt]/r_{17}^2$ where dM_{-4}/dt is the mass-loss rate in units of $10^{-4}\ M_\odot\ yr^{-1}$ and r_{17} is the distance from IRc2 in units of 10^{17} cm. If the fractional abundance of H_2O in the outflow is 1×10^{-4}, then the crossing rate of H_2O molecules is $1.5 \times 10^6\ [dM_{-4}/dt]/r_{17}^2\ cm^{-2}\ s^{-1}$. If this material is swept up into a volume of typical size a_{17} (in units of 10^{17} cm) along the path of the outflow, then the rate of increase of H_2O molecules $dn(H_2O)/dt$ (in units of $cm^{-3}\ s^{-1}$) is 1.5×10^{-11}

$[dM_{-4}/dt]/\{r_{17}^2 a_{17}\}$. For the compact ridge model, we take $dM_{-4}/dt = 1$, and $r_{17}^2 a_{17} = 80$, so that $dn(H_2O)/dt \approx 2 \times 10^{-13}$ cm^{-3} s^{-1}, which we refer to as the normal value of $dn(H_2O)/dt$, although we present detailed results for both a lower injection rate (6×10^{-14} cm^{-3} s^{-1}) and a higher injection rate (6×10^{-13} cm^{-3} s^{-1}). Note that we have assumed that this source term is independent of how distant the material in the compact ridge is from the outflow source, as long as the material is in the compact ridge. A more refined treatment would consist of dividing the material into slabs, with the source term diminishing for outer slabs more distant from IRc2 as the injected material is chemically processed. It is also of interest to note that the normal injection rate can also arise from evaporation of water off grain mantles if one assumes, for example, a mantle water concentration equivalent to a gas-phase concentration of ≈ 6 cm^{-3} evaporating over a time of 10^6 yr.

The results of four H_2O–injection models are shown at times of 5.0×10^5 yr, 7.9×10^5 yr, and 3.2×10^6 yr in Table 2 alongside the results of our unperturbed model, labeled Model 1. Models 2, 3, and 4 contain the lower, normal, and higher H_2O-injection rates respectively, whereas Model 5 has a normal injection rate which starts at $t = 0$. The chemical evolution times chosen for presentation in Table 2 are well past the standard peak abundance time ($1–2 \times 10^5$ yr) since H_2O injection in Models 2–4 starts at a time later than this ($t = 10^{13}$ s $\doteq 3.17 \times 10^5$ yr) and so that a sufficient amount of water injection can occur to influence the chemistry of Model 5 more than marginally. In this table we have chosen to tabulate absolute concentrations (in units of cm^{-3}) rather than fractional abundances, since the actual total abundance is changing, albeit slowly. Division of the results shown by $n(H_2) \approx 10^5$ cm^{-3} leads to approximate fractional abundances.

The rise in the water abundance injected into the source, labeled $(H_2O)_{mixed}$, can be followed in Table 2. The actual rise is considerably less than $(H_2O)_{mixed}$ because the injected water is chemically processed. For example, at 5.0×10^5 yr, the results of Model 3 show that while the water abundance has increased by a factor of about 4, or 0.2 cm^{-3}, with respect to Model 1, the total amount of water injected by this time is 1.2 cm^{-3}.

How does the rise in the water abundance affect the abundances of the oxygen-containing organic molecules? Our results show that while in all H_2O–injection models for $t < 3.2 \times 10^6$ yr the abundances of the oxygen-containing organic species tend to increase as a result of H_2O injection, in accord with the idea of Blake et al. (1987), the increase is far too small to explain the observed abundances. Indeed the enhancements are too small even to affect the normal time dependence for the abundances of these species, and they still peak at the so-called "early time" ($1–2 \times 10^5$ yr) of pseudo–time-dependent models. This can be seen in Figure 1, in which the fractional abundances of methanol and methyl formate are plotted as a function of time for Model 3, which contains the normal injection rate. The largest enhancements, up to one order of magnitude or so over the unperturbed model results, occur for Models 4 (rapid injection) and 5 (normal injection from $t = 0$). Consider, e.g., the case of methyl formate. At a time of 5×10^5 yr, when the unperturbed abundance is somewhat past its peak, the calculated enhancements are factors of 7.4 and 9.2 for Models 4 and 5, respectively, while at the later time of 7.9×10^5 yr, when the unperturbed methyl formate abundance has decreased strongly, the enhancements in these two models are factors of 8.2 and 4.9. At the unrealistically late time of 3.2×10^6 yr, when the injected water abundance corresponds to 54 cm^{-3} in Model 4, the abundance of methyl formate is actually greatest in the unperturbed model. Although enhancements of one order of magnitude can still occur at this time for other species, the unpertubed abundances are now so low that far greater enhancements are needed to reproduce observed abundances.

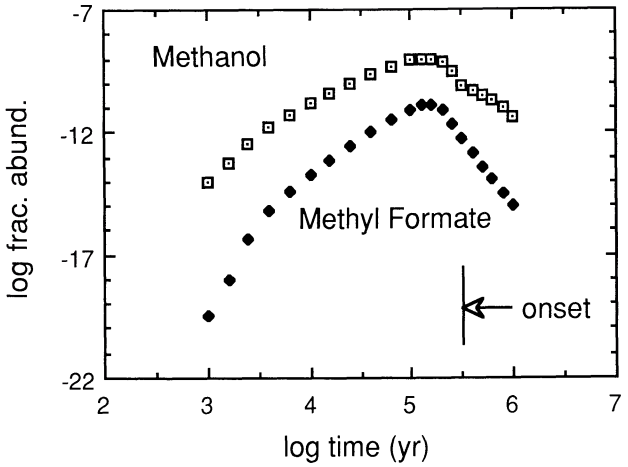

FIG. 1.—Calculated fractional abundances (with respect to H_2, which is assumed constant) of methanol (*open boxes*) and methyl formate (*black diamonds*) in Model 3 are plotted against time. The injection of water at the normal rate of 2×10^{-13} cm^{-3} s^{-1} commences at 10^{13} s. Only a small enhancement of the methanol abundance is observable.

The important quantitative result of Models 2–5 is thus that the increased H_2O abundance does not lead to a dramatic increase in the abundances of the oxygen-bearing organic molecules sufficient to explain the observed compact ridge abundances. At the injection rates considered, the injection of H_2O has a small effect on the formation of the larger species *basically because the water concentration, already large in the unperturbed model, does not increase sufficiently rapidly.* The injected H_2O reacts mainly with the species H_3^+ and HCO^+ (with rate coefficients much larger than that of the CH_3^+–H_2O radiative association) to form excess H_3O^+. The hydronium ions then recombine dissociatively with electrons to produce mainly the OH radical (Herd, Adams, & Smith 1990), which in turn produces increased abundances of O_2, NO, and CO_2 via neutral-neutral reactions with O, N, and CO, respectively, and alters the chemistry profoundly.

3.3. *Injection of Methanol*

Because the injection of H_2O at the rates we have considered does not appear to account for the oxygen-bearing organic molecules, the possibility that the injection of methanol influences these abundances is now considered. In the calculations below, it is assumed that CH_3OH is injected into the compact ridge at varying rates between 2×10^{-13} and 2×10^{-15} cm^{-3} s^{-1}. The origin of the methanol is unclear, since it has not been detected in an oxygen-rich circumstellar envelope, but it could arise from the evaporation of molecular ice mantles (Tielens & Allamandola 1987; Brown 1990) or from a methanol-rich gas such as observed in a variety of hot core-type objects (Menten et al. 1988). The results are listed as Models 6–9 in Table 3 for $t = 5.0 \times 10^5$ and 7.9×10^5 yr and compared with the unperturbed results (Model 1). The injected methanol concentration

TABLE 2

SELECTED ABUNDANCES (cm^{-3}) FOR WATER-INJECTION MODELS

Species	Model 1 unperturbed	Model 2 slow inj.	Model 3 normal inj.	Model 4 rapid inj.	Model 5 normal inj.
Inj. Rate (cm^{-3} s^{-1})	0.0	6.0(-14)	2.0(-13)	6.0(-13)	2.0(-13)
Inj. Time (yr)	----	3.2(+05)	3.2(+05)	3.2(+05)	0.0
	Abundances at 5.0 x 10^5 yr				
C	1.1(-04)	9.7(-05)	7.9(-05)	5.1(-05)	7.6(-05)
O	1.6(+01)	1.5(+01)	1.5(+01)	1.3(+01)	1.4(+01)
N	2.2(+00)	2.1(+00)	2.0(+00)	1.5(+00)	1.5(+00)
O_2	2.5(+00)	2.8(+00)	3.4(+00)	5.0(+00)	5.0(+00)
N_2	1.0(+00)	1.1(+00)	1.1(+00)	1.3(+00)	1.4(+00)
OH	1.3(-03)	1.5(-03)	2.0(-03)	3.6(-03)	2.4(-03)
CO	1.4(+01)	1.4(+01)	1.4(+01)	1.4(+01)	1.4(+01)
NO	9.2(-04)	1.1(-03)	1.4(-03)	2.5(-03)	1.7(-03)
H_2O	7.2(-02)	1.2(-01)	2.7(-01)	8.7(-01)	2.4(-01)
CO_2	1.2(-02)	1.2(-02)	1.4(-02)	1.7(-02)	2.3(-02)
H_2CO	1.3(-03)	1.4(-03)	1.5(-03)	2.1(-03)	2.2(-03)
CH_2CO	4.6(-04)	4.8(-04)	5.3(-04)	7.3(-04)	6.0(-04)
CH_3OH	1.1(-06)	1.8(-06)	3.3(-06)	8.9(-06)	5.7(-06)
CH_3CHO	2.8(-08)	3.5(-08)	5.5(-08)	1.4(-07)	7.1(-08)
$HCOOCH_3$	1.3(-09)	1.9(-09)	3.6(-09)	9.6(-09)	1.2(-08)
CH_3CH_2OH	6.0(-09)	7.5(-09)	1.2(-08)	2.8(-08)	2.1(-08)
CH_3OCH_3	1.7(-10)	2.0(-10)	2.6(-10)	4.3(-10)	1.0(-09)
CH_3COCH_3	1.4(-12)	2.3(-12)	2.5(-12)	4.0(-12)	3.9(-12)
$(H_2O)_{mixed}$	0.0	3.5(-01)	1.2(+00)	3.5(+00)	3.2(+00)
e	4.5(-03)	4.4(-03)	4.4(-03)	4.3(-03)	4.5(-03)
CH_3^+	3.0(-07)	2.7(-07)	2.3(-07)	1.5(-07)	2.6(-07)
H_3O^+	4.8(-05)	5.4(-05)	6.7(-05)	1.2(-04)	7.4(-05)
HCO^+	3.6(-04)	3.5(-04)	3.2(-04)	2.2(-04)	3.8(-04)
$CH_3OH_2^+$	7.1(-10)	1.1(-09)	1.9(-09)	4.0(-09)	3.0(-09)
	Abundances at 7.9 x 10^5 yr				
C	7.2(-06)	6.3(-06)	5.4(-06)	5.1(-06)	4.9(-06)
O	1.2(+01)	1.1(+01)	9.2(+00)	4.0(+00)	7.6(+00)
N	1.2(+00)	1.1(+00)	6.7(-01)	9.1(-02)	4.1(-01)
O_2	4.3(+00)	5.1(+00)	7.1(+00)	1.2(+01)	8.9(+00)
N_2	1.5(+00)	1.6(+00)	1.8(+00)	2.1(+00)	1.9(+00)
OH	1.5(-03)	1.9(-03)	3.1(-03)	1.1(-02)	3.8(-03)
CO	1.5(+01)	1.5(+01)	1.4(+01)	1.4(+01)	1.4(+01)
NO	1.1(-03)	1.4(-03)	2.2(-03)	7.3(-03)	2.7(-03)
H_2O	6.0(-02)	1.1(-01)	2.0(-01)	3.9(-01)	1.7(-01)
CO_2	7.8(-03)	9.3(-03)	1.2(-02)	2.1(-02)	2.1(-02)
H_2CO	4.4(-04)	4.9(-04)	6.0(-04)	8.7(-04)	9.6(-04)
CH_2CO	7.3(-05)	7.1(-05)	6.5(-05)	4.9(-05)	6.4(-05)

Species	Model 1 unperturbed	Model 2 slow inj.	Model 3 normal inj.	Model 4 rapid inj.	Model 5 normal inj.
Inj. Rate (cm^{-3} s^{-1})	0.0	6.0(-14)	2.0(-13)	6.0(-13)	2.0(-13)
Inj. Time (yr)	----	3.2(+05)	3.2(+05)	3.2(+05)	0.0
	Abundances at 7.9 x 10^5 yr (cont.)				
CH_3OH	3.5(-07)	5.8(-07)	9.8(-07)	1.5(-06)	8.4(-07)
CH_3CHO	5.5(-09)	6.3(-09)	8.2(-09)	1.3(-08)	7.1(-09)
$HCOOCH_3$	8.9(-11)	1.6(-10)	3.3(-10)	7.3(-10)	4.4(-10)
CH_3CH_2OH	3.8(-10)	4.9(-10)	7.4(-10)	1.2(-09)	9.8(-10)
CH_3OCH_3	3.0(-12)	4.4(-12)	6.6(-12)	9.1(-12)	7.1(-12)
CH_3COCH_3	8.8(-14)	9.5(-14)	1.1(-13)	1.2(-13)	9.5(-14)
$(H_2O)_{mixed}$	0.0	9.1(-01)	3.0(+00)	9.1(+00)	5.0(+00)
e	4.5(-03)	4.5(-03)	4.5(-03)	4.7(-03)	4.6(-03)
CH_3^+	1.4(-07)	1.3(-07)	1.1(-07)	8.7(-08)	1.4(-07)
H_3O^+	4.0(-05)	4.7(-05)	6.1(-05)	9.3(-05)	6.0(-05)
HCO^+	4.0(-04)	4.1(-04)	4.4(-04)	5.4(-04)	5.3(-04)
$CH_3OH_2^+$	2.6(-10)	4.2(-10)	7.3(-10)	1.2(-09)	7.4(-10)
	Abundances at 3.2 x 10^6 yr				
C	2.4(-07)	1.2(-07)	8.0(-08)	5.2(-08)	7.7(-08)
O	3.7(+00)	2.1(+00)	8.6(-01)	3.9(-03)	8.8(-01)
N	8.9(-02)	3.4(-02)	7.0(-03)	3.7(-05)	6.7(-03)
O_2	8.4(+00)	1.2(+01)	1.9(+01)	3.0(+01)	2.0(+01)
N_2	2.1(+00)	2.1(+00)	2.1(+00)	2.0(+00)	2.1(+00)
OH	2.8(-03)	5.9(-03)	2.1(-02)	5.8(+00)	2.1(-02)
CO	1.5(+01)	1.5(+01)	1.5(+01)	7.1(+00)	1.4(+01)
NO	2.0(-03)	4.1(-03)	1.4(-02)	2.8(-01)	1.4(-02)
H_2O	2.6(-02)	4.4(-02)	6.5(-02)	4.6(-01)	6.2(-02)
CO_2	9.5(-03)	1.9(-02)	6.3(-02)	7.4(+00)	6.5(-02)
H_2CO	1.0(-04)	1.1(-04)	1.0(-04)	3.0(-05)	1.1(-04)
CH_2CO	2.7(-06)	1.2(-06)	3.2(-07)	3.1(-08)	3.9(-07)
CH_3OH	5.3(-08)	4.8(-08)	2.3(-08)	4.3(-08)	1.9(-08)
CH_3CHO	3.7(-10)	1.8(-10)	6.8(-11)	4.9(-09)	7.5(-11)
$HCOOCH_3$	2.8(-12)	2.7(-12)	1.1(-12)	4.0(-13)	9.3(-13)
CH_3CH_2OH	6.8(-12)	3.7(-12)	1.0(-12)	9.9(-11)	1.1(-12)
CH_3OCH_3	1.1(-13)	5.3(-14)	8.3(-15)	2.9(-15)	6.0(-15)
CH_3COCH_3	2.0(-15)	5.3(-16)	6.5(-17)	7.5(-16)	6.3(-17)
$(H_2O)_{mixed}$	0.0	5.4(+00)	1.8(+01)	5.4(+01)	2.0(+01)
e	4.6(-03)	4.8(-03)	5.4(-03)	5.3(-03)	5.5(-03)
CH_3^+	6.6(-08)	4.9(-08)	2.5(-08)	3.6(-09)	2.3(-08)
H_3O^+	2.0(-05)	2.4(-05)	3.2(-05)	3.5(-04)	3.2(-05)
HCO^+	5.0(-04)	7.2(-04)	1.2(-03)	5.3(-04)	1.2(-03)
$CH_3OH_2^+$	4.9(-11)	5.9(-11)	4.1(-11)	4.3(-11)	3.6(-11)

NOTE.—Abundances are given in the form $a(-b)$, where $a(-b)$ stands for $a \times 10^{-b}$.

is labeled $(CH_3OH)_{mixed}$. Models 6 and 7 have methanol injection rates of 6×10^{-14} and 2×10^{-13} cm^{-3} s^{-1}, respectively, starting at $t = 10^{13}$ s, while Model 8 has an injection rate of 2×10^{-13} cm^{-3} s^{-1} but starting at $t = 0$. As with water, the lower of the two rates is called "slow injection" in the table, while the higher of the two is called "normal injection." Model 9 contains a very much slower injection rate of 2×10^{-15} cm^{-3} s^{-1} for reasons discussed below.

At 5.0×10^5 yr, the methanol abundance in Model 6 (which contains the "slow" injection rate) has already risen by five orders of magnitude over the (small) unperturbed value and is even somewhat larger than the observed abundance. The injected methanol proton transfers with species such as H_3^+, HCO^+, and H_3O^+ to form $CH_3OH_2^+$, leading to a similar rise in the abundance of this ion. Subsequent reactions of $CH_3OH_2^+$ with H_2CO and with CH_3OH lead to the formation of methyl formate ($HCOOCH_3$) and dimethyl ether (CH_3OCH_3) via reactions (2) and (3), respectively. In addition, the radiative association between CH_3^+ and CH_3OH, reaction (4), also contributes significantly to the formation of CH_3OCH_3. The calculated abundances of methyl formate and dimethyl ether at 5.0×10^5 yr in Model 6 are enhanced by over five orders of magnitude from their unperturbed values and are in good agreement with observed abundances. Moreover, the

TABLE 3

SELECTED ABUNDANCES (cm^{-3}) FOR METHANOL-INJECTION MODELS

	Model 1 unperturbed	Model 6 slow inj.	Model 7 normal inj.	Model 8 normal inj.	Model 9 very slow
Inj. Rate (cm^{-3} s^{-1})	0.0	6.0(-14)	2.0(-13)	2.0(-13)	2.0(-15)
Inj. Time (yr)	----	3.2(+05)	3.2(+05)	0.0	3.2(+05)
Species	Abundances at 5.0 x 10^5 yr				
C	1.1(-04)	2.2(-04)	3.4(-04)	3.2(-04)	1.1(-04)
O	1.6(+01)	1.5(+01)	1.4(+01)	1.2(+01)	1.5(+01)
N	2.2(+00)	2.2(+00)	2.1(+00)	1.7(+00)	2.2(+00)
O_2	2.5(+00)	2.7(+00)	3.0(+00)	4.2(+00)	2.6(+00)
N_2	1.0(+00)	1.0(+00)	1.1(+00)	1.3(+00)	1.0(+00)
OH	1.3(-03)	1.4(-03)	1.7(-03)	2.3(-03)	1.4(-03)
CO	1.4(+01)	1.5(+01)	1.4(+01)	1.6(+01)	1.4(+01)
NO	9.2(-04)	1.0(-03)	1.2(-03)	1.6(-03)	1.0(-03)
H_2O	7.2(-02)	1.2(-01)	2.5(-01)	3.8(-01)	7.3(-02)
CO_2	1.2(-02)	4.3(-02)	1.0(-01)	3.6(-01)	1.3(-02)
H_2CO	1.3(-03)	4.7(-02)	1.6(-01)	2.6(-01)	2.7(-03)
CH_2CO	4.6(-04)	5.5(-04)	7.7(-04)	2.5(-03)	4.3(-04)
CH_3OH	1.1(-06)	1.1(-01)	4.8(-01)	7.1(-01)	3.1(-03)
CH_3CHO	2.8(-08)	3.8(-08)	6.5(-08)	3.2(-07)	2.6(-08)
$HCOOCH_3$	1.3(-09)	8.0(-04)	8.5(-03)	2.7(-02)	1.7(-06)
CH_3CH_2OH	6.0(-09)	9.8(-09)	2.0(-08)	1.4(-07)	5.7(-09)
CH_3OCH_3	1.7(-10)	1.1(-03)	1.4(-02)	4.4(-02)	1.1(-06)
CH_3COCH_3	1.4(-12)	3.9(-12)	1.2(-11)	1.1(-10)	1.3(-12)
$(CH_3OH)_{mixed}$	0.0	3.5(-01)	1.2(+00)	3.2(+00)	1.2(-02)
e	4.5(-03)	4.4(-03)	4.3(-03)	4.4(-03)	4.5(-03)
CH_3^+	3.0(-07)	6.7(-07)	1.1(-06)	1.1(-06)	3.1(-07)
H_3O^+	4.8(-05)	5.0(-05)	5.5(-05)	6.0(-05)	5.1(-05)
HCO^+	3.6(-04)	3.0(-04)	2.0(-04)	1.8(-04)	4.0(-04)
$CH_3OH_2^+$	7.1(-10)	3.1(-05)	8.3(-05)	1.1(-04)	1.1(-06)
Species	Abundances at 7.9 x 10^5 yr				
C	7.2(-06)	5.0(-05)	1.0(-04)	8.6(-05)	6.3(-06)
O	1.2(+01)	1.0(+01)	7.1(+00)	4.8(+00)	1.1(+01)
N	1.2(+00)	1.1(+00)	6.9(-01)	4.1(-01)	1.1(+00)
O_2	4.3(+00)	5.0(+00)	6.3(+00)	7.6(+00)	4.8(+00)
N_2	1.5(+00)	1.6(+00)	1.7(+00)	1.9(+00)	1.6(+00)
OH	1.5(-03)	1.9(-03)	3.2(-03)	5.0(-03)	1.9(-03)
CO	1.5(+01)	1.5(+01)	1.6(+01)	1.8(+01)	1.5(+01)
NO	1.1(-03)	1.4(-03)	2.3(-03)	3.5(-03)	1.4(-03)
H_2O	6.0(-02)	1.1(-01)	3.1(-01)	2.8(-01)	5.7(-02)
CO_2	7.8(-03)	1.1(-01)	3.5(-01)	6.4(-01)	1.1(-02)
H_2CO	4.4(-04)	5.5(-02)	2.3(-01)	2.3(-01)	1.8(-03)
CH_2CO	7.3(-05)	1.1(-04)	2.2(-04)	4.0(-04)	5.6(-05)
CH_3OH	3.5(-07)	1.2(-01)	6.0(-01)	5.6(-01)	2.9(-03)
CH_3CHO	5.5(-09)	9.3(-09)	2.7(-08)	5.3(-08)	3.9(-09)
$HCOOCH_3$	8.9(-11)	1.4(-03)	2.4(-02)	2.7(-02)	1.3(-06)
CH_3CH_2OH	3.8(-10)	1.8(-09)	1.1(-08)	2.7(-08)	2.8(-10)
CH_3OCH_3	3.0(-12)	1.9(-03)	3.8(-02)	4.2(-02)	1.2(-06)
CH_3COCH_3	8.8(-14)	5.4(-13)	4.1(-12)	9.6(-12)	5.4(-14)
$(CH_3OH)_{mixed}$	0.0	9.1(-01)	3.0(+00)	5.0(+00)	3.0(-02)
e	4.5(-03)	4.5(-03)	4.4(-03)	4.5(-03)	4.6(-03)
CH_3^+	1.4(-07)	1.8(-07)	8.8(-07)	8.5(-07)	1.5(-07)
H_3O^+	4.0(-05)	4.3(-05)	4.9(-05)	4.5(-05)	4.6(-05)
HCO^+	4.0(-04)	3.5(-04)	2.2(-04)	2.8(-04)	5.1(-04)
$CH_3OH_2^+$	2.6(-10)	3.8(-05)	1.1(-04)	1.3(-04)	1.3(-06)

NOTE.—Abundances are given in the form $a(-b)$, where $a(-b)$ stands for $a \times 10^{-b}$.

TABLE 4

COMPARISON OF CALCULATED FRACTIONAL ABUNDANCES OF MODEL 6 WITH OBSERVED COMPACT RIDGE VALUES

SPECIES	FRACTIONAL ABUNDANCES		
	5.0×10^5 yr[a]	7.9×10^5 yr[a]	Observed[b]
H_2CO	4.7(−07)	5.5(−07)	4(−08)[c]
CH_2CO	5.5(−09)	1.1(−09)	7(−10)
CH_3OH	1.1(−06)	1.2(−06)	1(−07)
$HCOOCH_3$	8.0(−09)	1.4(−08)	9(−09)
CH_3OCH_3	1.1(−08)	1.9(−08)	1(−08)
CH_3CHO	3.8(−13)	9.3(−14)	<2(−10)
CH_3CH_2OH	9.8(−14)	1.8(−14)	<5(−10)

NOTE.—Abundances are given in the form $a(-b)$, where $a(-b)$ stands for $a \times 10^{-b}$.

[a] With respect to $H_2 \approx 1(+05)$ cm^{-3}.

[b] Blake et al. (1987) unless otherwise noted.

[c] Magnum et al. (1990).

abundances of other oxygen-bearing organic molecules such as acetaldehyde (CH_3CHO), ethanol (CH_3CH_2OH), and acetone (CH_3COCH_3), the formation routes of which do not involve methanol or its protonated ion, are enhanced to a much smaller degree and are still in good accord with the negative observations. Table 4 contains a comparison of Model 6 results at 5×10^5 yr and observed compact ridge values for the fractional abundances of all oxygen-containing organic molecules. The level of agreement is within one order of magnitude for all species except formaldehyde (H_2CO) which is overproduced by a factor of 12. Models 7 and 8 contain even larger enhancements for methanol, methyl formate, and dimethyl ether 5×10^5 yr than does Model 6. At the later time of 7.9×10^5 yr, these three molecules remain pretty much at their previous abundances in Models 6–8, so that the time dependence is not crucial. Model 6 results at this later time are also included as fractional abundances in Table 4, where the agreement with observation is seen to be as good as for the earlier time. The dramatic enhancements in the methanol and methyl formate abundances for Model 6 at times after methanol injection commences are depicted in Figure 2.

Since Models 6–8 correspond to mixing in a fractional abundance of CH_3OH with respect to H_2 of $(3–10) \times 10^{-5}$ *if the source of the methanol is an* H_2*–dominated wind and not grain desorption*, which is far larger than the known gas-phase abundance of this trace species in any source, we have performed one calculation (Model 9) for a much lower mixing rate of 2×10^{-15} cm^{-3} s^{-1} for $t \geq 10^{13}$ s, corresponding to a fractional abundance of 10^{-6}. This is more typical of the methanol calculated for hot core-type regions (Menten et al. 1988) in which the gas-phase composition reflects grain mantle compositions prior to a rapid evaporation process (Brown et al. 1988; Brown & Millar 1989a, b). The results of this calculation, given in Table 3, show that by 5×10^5 yr, the methanol abundance has increased relative to its unperturbed value by over three orders of magnitude and has reached a fractional abundance of 3×10^{-8}, only slightly below that observed (Table 1). The methyl formate abundance also rises by three orders of magnitude to the fractional abundance of 2×10^{-11}. This value, which remains relatively constant through 7.9×10^5 yr, is comparable to the peak unperturbed abundance, which is still three orders of magnitude below the observed value. The fractional abundance of dimethyl ether, enhanced by four orders of magnitude at 5×10^5 yr, is 1×10^{-11} which, although more than one order of magnitude larger than the peak unperturbed abundance, is still three orders of magnitude below the observed value. At the later time of 7.9×10^5 yr, the calculated dimethyl ether abundance in Model 9 remains the same. Thus, although the low methanol injection model is successful in reproducing the observed methanol abundance, it cannot reproduce the observed abundances of the two more complex species produced from methanol.

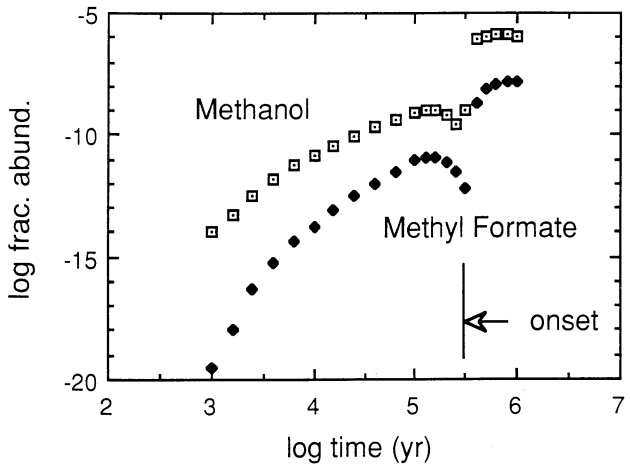

FIG. 2.—Same plot as shown in Fig. 1 but for Model 6, in which methanol is injected into the compact ridge at a rate of 6×10^{-14} cm^{-3} s^{-1}. Here both the methanol and methyl formate abundances increase dramatically and remain at their high levels.

4. CONCLUSIONS

It has been suggested by Blake et al. (1987) that the unique chemistry of the compact ridge source in Orion might be explained by the infusion of material rich in water from the IRc2 outflow. According to these authors, the water reacts with methyl ion to form protonated methanol (reaction [1]), and subsequent reactions lead to large abundances of methanol, methyl formate, and dimethyl ether, the abundances of which are greatly enhanced in the compact ridge. We have attempted to test this idea via quantitative model calculations. The injection of water has been simulated by a simple model in which one common injection rate pertains to the whole source and, in the absence of chemical processing, leads to a water concentration that increases linearly with time. Although an estimated mass-loss rate from IRc2 and geometrical arguments were utilized to calculate a water injection rate of 2×10^{-13} cm^{-3} s^{-1} we have also run models with lower and higher injection rates. In addition, the starting time of the water injection has been varied. In most of our models, it has been turned on at $t = 10^{13}$ s (3.17×10^5 yr) after the gas-phase chemistry itself onsets. This time delay is reasonable because of the need for sufficient time for both the formation of the source IRc2 from its precursor dense cloud material and the transit of its wind to the compact ridge. However, we have also run models in which the water injection is turned on at earlier times, and we explicitly present results for a turn-on time $t = 0$ s. The gas-phase chemistry is treated by our customary pseudo–time-dependent approach (Millar et al. 1987), modified to include the chemistry of oxygen-containing organic species and to include a term for water injection.

In all of our water injection models, only small enhancements in the abundances of methanol, methyl formate, and dimethyl ether are calculated compared with a model in which

there is no water injection. The enhancements (≤ 1 magnitude) are not large enough to account for the observed abundances of these three species in the compact ridge, nor do they even change the standard time dependence of the abundances calculated in pseudo–time-dependent models, in which peak abundances occur at times between $1–2 \times 10^5$ yr. Given the physical simplicity of our models and the uncertainties in key rate coefficients such as that for the critical radiative association between CH_3^+ and H_2O, it is not possible to reject entirely the appealing picture of Blake et al. (1987). Still, our calculations do not support this picture. The basic chemical problems are that (*a*) the conversion of water into methanol and more complex species is inefficient because of the slowness of the primary CH_3^+–H_2O radiative association and the low abundance of the methyl ion vis-a-vis other reactant ions, and (*b*) there is relatively small change in the water abundance compared with the change of the methanol abundance in methanol-injection models.

To determine if a much larger water inflow could change our conclusions, we have run a model in which the water injection rate is 3×10^{-12} cm^{-3} s^{-1}, over one order of magnitude faster than our standard rate, and in which the injection commences at $t = 0$. Such an injection rate would require a mass loss of over 100 $M_\odot$ from IRc2 in 10^5 yr with our assumptions. Alternatively, it could be accounted for by the desorption of water-rich grain mantles with a water concentration equivalent to the rather large gas phase concentration of 10 cm^{-3} in a similar time period. We note in this context that Magnum et al. (1990) argue for a modest enhancement in the abundance of H_2CO in the compact ridge cloud and suggest that it is due to grain mantle evaporation due to heating from an internal object perhaps associated with a known compact 2 cm continuum source (Churchwell et al. 1987). In the rapid water injection model, the peak fractional abundances of methanol, methyl formate, and dimethyl ether, which occur at the standard time of $1–2 \times 10^5$ yr, are 3×10^{-8}, 3×10^{-10}, and 1×10^{-11}, respectively. Although the enhanced peak fractional abundance of methanol is near the observed value (Table 1) of 10^{-7}, the enhanced peak fractional abundances of methyl formate and dimethyl ether are still factors of 30 and 1000 below their observed values. All other species in the model have abundances that differ only slightly from their unperturbed values. An even larger (and possibly more unphysical) water injection rate appears to be required!

One valid criticism of our standard model is that it does not account for the much larger gas density ($n \approx 10^6$–10^7 cm^{-3}) of the compact ridge compared with the more extended cloud ($n \approx 2 \times 10^5$ cm^{-3}). At our standard water-injection rate of 2×10^{-13} cm^{-3} s^{-1} and water/H_2 abundance ratio of 10^{-4} in the outflow material, the H_2 density merely doubles its initial value of 10^5 cm^{-3} at an unphysically long time of more than 10^6 yr. Even with the very high injection rate of 3×10^{-12} cm^{-3} s^{-1}, a gas density of 10^6 cm^{-3} cannot be achieved in under 10^6 yr. Gas density increases due to gravitational collapse are an integral part of current hot core models (Brown et al. 1988; Brown & Millar 1989a, b) and should perhaps be considered here as well. More physically complex models of the IRc2 outflow—compact ridge cloud interaction may also be helpful.

It is also possible that we have failed to include all of the relevant gas phase reactions leading to oxygen-containing organic molecules. A particular source of uncertainty are reactions between hydrocarbon ions and oxygen atoms, few of which have been studied in the laboratory. It is possible that these lead to oxygenated hydrocarbon ions which are precursors to oxygenated neutral organics. We have included only one such reaction (reaction [9]) in our model. Inclusion of more such reactions might boost the unperturbed abundances of the oxygen-containing organic species and lessen the need for such large enhancements to account for the observations. An outflow rich in atomic oxygen might also be a source of enhanced abundances for oxygen-containing organic species.

Given the failure of our water-injection models to account for the enhanced abundances of methanol, methyl formate, and dimethyl ether in the compact ridge, we have also run models in which methanol is injected directly. This is clearly a much more efficient procedure for producing more complex molecules, although the source of the injected methanol can only be conjectured; evaporated oxygen-rich local grain mantles (Brown 1990) are one possibility, injection of a methanol-rich hot core-type gas is a second (Menten et al. 1988). In any case, one of our methanol-injection models (Model 6) is reasonably successful in explaining the observed abundances of oxygen-containing organic species—both those enhanced greatly over their unperturbed values and those not so enhanced—for time periods from $5–10 \times 10^5$ yr after the onset of the gas-phase chemistry. The methanol injection rate of 6×10^{-14} cm^{-3} s^{-1} in this model can be maintained for the necessary period by an evaporation process if the number of methanol molecules initially in grain mantles corresponds to a gas-phase abundance of ≈ 1 cm^{-3}, a number roughly achievable in some grain model calculations (Brown 1990).

The results of Model 6 shows surprisingly few abundance gradients from normal unperturbed results. One exception is CO_2, which is enhanced by factors of 4–10 depending on the time. The major gas-phase reaction for the production of CO_2 has been put into some doubt, however, at low temperature (Smith 1988). Moreover, Minh, Irvine, & Ziurys (1988) did not detect $HOCO^+$ towards Orion KL. Another strong prediction of this model is a high fractional abundance ($> 10^{-10}$) for protonated methanol, the rotational spectrum of which has yet to be identified in the laboratory. The predictions of the methanol-injection models must be treated cautiously, since the reaction set may not be large enough to treat adequately all the possible ramifications of such a large methanol abundance and since, if large amounts of methanol are being injected into the compact ridge gas, in all probability other molecules are also being injected. Indeed, an interesting topic for future work might be the injection of a variety of molecules thought to be produced on oxygen-rich grain mantles (Brown 1990).

S. B. C. acknowledges partial support of the US Air Force under Grant AFOSR-89-0194. E. H. acknowledges the National Science Foundation for support of his theoretical program via grant AST-8915190. T. M. acknowledges the Science and Engineering Research Council (SERC) (UK) for support of this work.

REFERENCES

Bass, L. M., Cates, R. D., Jarrold, M. F., Kirchner, N. J., & Bowers, M. T. 1983, JACS, 105, 7024
Bates, D. R., & Herbst, E. 1988, in Rate Coefficients in Astrochemstry, ed. T. J. Millar and D. A. Williams (Dordrecht: Kluwer), p. 17
Blake, G. A., Sutton, E. C., Masson, C. R., & Phillips, T. G. 1987, ApJ, 315, 621
Bohme, D. K. 1990, private communication
Brown, P. D. 1990, MNRAS, 243, 65
Brown, P. D., Charnley, S. B., & Millar, T. J. 1988, MNRAS, 231, 409

Brown, P. D., & Millar, T. J. 1989a, MNRAS, 237, 661
———. 1989b, MNRAS, 240, 25P
Churchwell, E. B., Felli, M., Wood, D. O. S., & Massi, M. 1987, ApJ, 321, 516
Combes, F., Gerin, M., Wootten, A., Wlodarczak, G., Clausset, F., & Encrenaz, P. J. 1987, A&A, 180, L13
Gerlich, D., & Kaefer, G. 1989, ApJ, 347, 849
Green, S., & Herbst, E. 1979, ApJ, 229, 121
Henkel, C., Mauersberger, R., Wilson, T. L., Snyder, L. E., Menten, K., & Wouterloot, J. G. A. 1987, A&A, 182, 299
Herbst, E. 1985, ApJ, 291, 226
———. 1987, ApJ, 313, 867
———. 1988, in Dissociative Recombination: Theory, Experiment and Applications, ed. J. B. A. Mitchell & S. L. Guberman (Singapore: World Scientific), p. 303
Herbst, E., Giles, K., & Smith, D. 1990, ApJ, 358, 468
Herbst, E., & Leung, C. M. 1989, ApJS, 69, 271
———. 1990, A&A, 233, 177
Herbst, E., Smith, D., Adams, N. G., & McIntosh, B. J. 1989, J. Chem. Soc. Faraday Trans, 2, 85, 1655
Herd, C. R., Adams, N. G., & Smith, D. 1990, ApJ, 349, 388
Ikezoe, Y., Matsuoka, S., Takebe, M., & Viggiano, A. 1987, Gas Phase Ion-Molecule Reaction Rate Coefficients Through 1986 (Tokyo: Maruzen Co.)
Irvine, W. M., Goldsmith, P. F., & Hjalmarson, Å. 1987, in Interstellar Processes, ed. D. J. Hollenbach & H. A. Thronson, Jr. (Dordrecht: Reidel), p. 561
Jacq, T., Walmsley, C. M., Henkel, C., Baudry, A., Mauersberger, R., & Jewell, P. R. 1990, A&A, 228, 447
Langer, W. D. and Glassgold, A. E. 1990, ApJ, 351, 123
Magnum, J. G., Wootten, A., Loren, R. B., & Wadiak, E. J. 1990, ApJ, 348, 556
Menten, K. M., Walmsley, C. M., Henkel, C., & Wilson, T. L. 1988, A&A, 198, 253
Millar, T. J., DeFrees, D. J., McLean, A. D., & Herbst, E. 1988, A&A, 194, 250
Millar, T. J., Leung, C. M., & Herbst, E. 1987, A&A, 183, 109
Minh, Y. C., Irvine, W. M., & Ziurys, L. M. 1988, ApJ, 334, 175
Pauls, T. A., Wilson, T. L., Bieging, J. H., & Martin, R. N. 1983, A&A, 124, 23
Smith, D., & Adams, N. G. 1978, ApJ, 220, L87
Smith, I. M. W. 1988, MNRAS, 234, 1059
———. 1989, ApJ, 347, 282
Sweitzer, J. S. 1978, ApJ, 225, 116
Tielens, A. G. G. M., & Allamandola, L. J. 1987, in Interstellar Processes, ed. D. J. Hollenbach & H. A. Thronson, Jr. (Dordrecht: Reidel), p. 397
Walmsley, C. M. 1989, in Interstellar Dust, ed. L. J. Allamandola & A. G. G. M. Tielens (Dordrecht: Kluwer), p. 263
Walmsley, C. M., Hersen, W., Henkel, C., Mauersberger, R., & Wilson, T. L. 1987, A&A, 172, 311
Wlodek, S., Bohme, D. K., & Herbst, E. 1990, MNRAS, 242, 674
Wynn-Williams, C. G., Genzel, R., Becklin, E. E., & Downes, D. 1984, ApJ, 281, 172